Broadband Tuneable Travelling Wave Parametric Multiplier based on High-gap Superconducting Thin Film

Boon-Kok Tan[a*], Nikita Klimovich[a], and Peter K. Day[b]

[a]Dept. of Physics (Astrophysics), Univ. of Oxford, DWB Keble Road, OX1 3RH, Oxford, U.K.
[b]Jet Propulsion Laboratory (NASA), 4800 Oak Grove Dr., Pasadena 91109, CA, USA.

ABSTRACT

The well-established technology of the superconducting quantum parametric amplifier (SPA) can be reconfigured to perform functions beyond amplification, such as frequency multiplication, by utilising the low-noise, low-loss superconducting nonlinear transmission line. This versatile technology holds potential for various applications, including 'pumping' a millimetre (mm) or sub-mm wave heterodyne mixer or driving a high-frequency SPA. Its significance lies in the ability to incorporate a high-purity signal source into the cryogenic stage alongside the primary detector, thereby eliminating noise associated with room temperature sources. Additionally, there is potential for on-chip integration with the detector circuit, leading to a more compact architecture.

This manuscript details the design of a travelling-wave parametric multiplier (TWPaM) that exploits the nonlinear wave-mixing mechanism to enhance the third harmonic growth from a strong pump tone injected into the travelling wave parametric amplifier (TWPA)-like device. While this functionality has been demonstrated previously, it exhibited narrowband performance. In this manuscript, we present our approach to designing a dispersion engineering scheme that enables the generation of broadband tunable tripler tones with high conversion efficiency. We showcase our design methodology using a niobium titanium nitride (NbTiN) high-gap thin-film transmission line as an example. Our presentation includes the theoretical model governing the physics of higher harmonics generation, emphasising phase-matching conditions that allow for broadband operation while suppressing unwanted modes. Although the ultimate aim is to develop a mm/sub-mm TWPaM, we aim to demonstrate the feasibility of their operation with a scaled microwave design in this manuscript. We will show that we can theoretically achieve close to 35% conversion efficiency across approximately 60% operational bandwidth.

Keywords: Broadband, Frequency Multiplier, Harmonics Generation, Tunability, Parametric Amplifier, Wave-mixing, Nonlinear superconducting medium, Microwave, Millimetre/Sub-Millimetre

1. INTRODUCTION

The generation of high-frequency signal tones with high purity and low noise properties is crucial for many applications. Traditionally, this has been achieved using a chain of frequency up-converters, which utilise semiconductor diodes and waveguide structures in conjunction with a microwave source.[1,2] Although these solutions manage to achieve high conversion efficiency over a broad bandwidth, they are bulky and struggle to achieve quantum-limited noise performance. Additionally, they are challenging to incorporate into the cryogenic environment where ultra-sensitive detectors operate and difficult to integrate on-chip with detector circuits.

In contrast, superconducting travelling wave parametric amplifier (TWPA) technology is renowned for achieving broadband amplification with quantum-limited noise performance.[3,4] TWPA technology is also known for its adaptability. With adequate design and innovation, it can be reconfigured to serve other functions, such as quantum-limited frequency up- and down-conversion processes, by leveraging the low-noise, low-loss superconducting nonlinear transmission line.[5,6] For example, the frequency multiplication capability benefits applications ranging from 'pumping' millimetre (mm) and sub-millimetre (sub-mm) heterodyne receivers to driving high-frequency parametric quantum amplifiers. This offers a high-purity, ultra-low noise signal source at the cryogenic stage, with minimal thermal noise.

*E-mail: boonkok.tan@physics.ox.ac.uk

This paper introduces a travelling-wave parametric multiplier (TWPaM, pronounced "*too-pam*") design, utilising the nonlinear wave-mixing mechanism for the operation of a broadband tunable tripler with high conversion efficiency. We use a niobium titanium nitride (NbTiN) kinetic-inductance based TWPaM as an example to showcase the methodology. The same theoretical framework could be applied to Josephson junction-based devices,[7] including SQUID (Superconducting Quantum Interference Device)[8] and SNAIL (Superconducting Nonlinear Asymmetric Inductive Element)[9] devices.

2. THEORETICAL MODEL

Here, we derive the coupled wave equations (CME) for the TWPaM in the tripler mode. The nonlinear wave equation for a highly nonlinear long transmission line can be described as follows:[10]

$$\frac{\partial^2 I}{\partial z^2} - RG \cdot I(z,t) - (RC + LG)\frac{\partial I(z,t)}{\partial t} - L_0 C \frac{\partial^2 I}{\partial t^2} - \frac{\beta_{nl} L_0 C}{I_C^2}\frac{\partial}{\partial t}\left(I^2 \frac{\partial I}{\partial t}\right) = 0 \tag{1}$$

where R, L, G and C are the series resistance, inductance and shunt conductance and capacitance, I is the propagating current tones, L_0 is the zero-current kinetic inductance and β_{nl} is the constant defining the origin of nonlinearity of the transmission line[11] ($\beta_{nl} = 1$ for kinetic inductance and 0.5 for junction-based nonlinear transmission line).

Taking the ansatz that the solutions will be forward propagating waves of the form:

$$I = \tfrac{1}{2}[A_p(z)e^{(i\omega_p t - \gamma_p z)} + A_{3p}(z)e^{(i\omega_{3p} t - \gamma_{3p} z)} + A_{5p}(z)e^{(i\omega_{5p} t - \gamma_{5p} z)} + A_{7p}(z)e^{(i\omega_{7p} t - \gamma_{7p} z)} + A_{9p}(z)e^{(i\omega_{9p} t - \gamma_{9p} z)} + \text{c.c.}], \tag{2}$$

$$\text{or} \quad I = \tfrac{1}{2}A_m(z)e^{(i\omega_m t - \gamma_m z)} + \text{c.c.} \quad \text{where} \quad m = p, 3p, 5p, 7p, 9p..., \tag{3}$$

where A_m are the slowly varying amplitude of the waves, $\gamma_m = \alpha_m + i\beta m = \sqrt{(R + i\omega_m L)(G + i\omega_m C)}$ the complex propagation constant, α_m the attenuation constant, β_m the phase constant or wave vector in pure TEM mode, and ω_m the angular frequencies. In this example, we truncated our derivation at 9^{th} harmonics.

Neglecting the second derivatives of the slowly varying amplitudes using the slowly varying envelope approximation: $\left|\frac{d^2 A_m}{dx^2}\right| \ll \left|k_m \frac{dA_m}{dx}\right|$; and the first derivatives of the slowly varying amplitudes on the right side of the nonlinear wave equation: $\left|\frac{dA_m}{dx}\right| \ll |k_m A_m|$; and substituting the input field Eq. 3 into the nonlinear transmission line equation Eq. 1 results in:

$$-\gamma_m \frac{\partial A_m(z)}{\partial z} e^{(i\omega_m t - \gamma_m z)} = \frac{\beta_{nl} L_0 C}{I_C^2}\frac{\partial}{\partial t}\left(I^2 \frac{\partial I}{\partial t}\right) \tag{4}$$

Separating out the terms that oscillate at the pumps, the third, fifth, seventh and ninth harmonic frequencies, and solved for each tones, we get the following set of coupled equations (assuming $\alpha_m = 0$ for lossless superconducting transmission line):

$$\begin{aligned}
\gamma_p \frac{\partial A_p(z)}{\partial z} = \frac{\beta_{nl}\beta_p^2}{8 I_C^2}\Big[& A_p A_p^* A_p + 2A_{3p}A_{3p}^* A_p + 2A_{5p}A_{5p}^* A_p + 2A_{7p}A_{7p}^* A_p + 2A_{9p}A_{9p}^* A_p \\
& + A_p^{*2} A_{3p} e^{-(3\beta_p - \beta_{3p})} + A_{3p}^2 A_{5p}^* e^{(-\beta_p + 2\beta_{3p} - \beta_{5p})} \\
& + A_{3p}^{*2} A_{7p}^* e^{(-\beta_p - 2\beta_{3p} + \beta_{7p})} + A_{5p}^2 A_{9p}^* e^{(-\beta_p + 2\beta_{5p} - \beta_{9p})} \\
& + 2A_p^* A_{3p}^* A_{5p} e^{(-2\beta_p - \beta_{3p} + \beta_{5p})} + 2A_p^* A_{5p}^* A_{7p} e^{(-2\beta_p - \beta_{5p} + \beta_{7p})} + 2A_p^* A_{7p}^* A_{9p} e^{(-2\beta_p - \beta_{7p} + \beta_{9p})} \\
& + 2A_{3p}^* A_{5p}^* A_{9p} e^{(-\beta_p - \beta_{3p} - \beta_{5p} + \beta_{9p})} + 2A_{3p} A_{5p} A_{7p}^* e^{(-\beta_p + \beta_{3p} + \beta_{5p} - \beta_{7p})} \\
& + 2A_{3p} A_{7p} A_{9p}^* e^{(-\beta_p + \beta_{3p} + \beta_{7p} - \beta_{9p})}\Big]
\end{aligned}$$

$$
\begin{aligned}
\gamma_{3p}\frac{\partial A_{3p}(z)}{\partial z} = \frac{\beta_{nl}\beta_{3p}^2}{8I_C^2}\Big[&2A_pA_p^*A_{3p} + A_{3p}A_{3p}^*A_{3p} + 2A_{5p}A_{5p}^*A_{3p} + 2A_{7p}A_{7p}^*A_{3p} + 2A_{9p}A_{9p}^*A_{3p}\\
&+ A_p^{*2}A_{5p}e^{(-2\beta_p-\beta_{3p}+\beta_{5p})} + A_{3p}^{*2}A_{9p}e^{(-2\beta_{3p}-\beta_{3p}+\beta_{9p})} + A_{5p}^2A_{7p}^*e^{(2\beta_{5p}-\beta_{3p}-\beta_{7p})}\\
&+ 2A_pA_{3p}^*A_{5p}e^{(\beta_p-2\beta_{3p}+\beta_{5p})} + 2A_p^*A_{3p}^*A_{7p}e^{(-\beta_p-2\beta_{3p}+\beta_{7p})} + 2A_pA_{5p}^*A_{7p}e^{(\beta_p-\beta_{3p}-\beta_{5p}+\beta_{7p})}\\
&+ 2A_p^*A_{5p}^*A_{9p}e^{(-\beta_p-\beta_{3p}-\beta_{5p}+\beta_{9p})} + 2A_pA_{7p}^*A_{9p}e^{(\beta_p-\beta_{3p}-\beta_{7p}+\beta_{9p})} + 2A_{5p}A_{7p}A_{9p}^*e^{(-\beta_{3p}+\beta_{5p}+\beta_{7p}-\beta_{9p})}\\
&+ \frac{1}{3}A_p^3e^{(3\beta_p-\beta_{3p})}\Big]\\
\gamma_{5p}\frac{\partial A_{5p}(z)}{\partial z} = \frac{\beta_{nl}\beta_{5p}^2}{8I_C^2}\Big[&2A_pA_p^*A_{5p} + 2A_{3p}A_{3p}^*A_{5p} + A_{5p}A_{5p}^*A_{5p} + 2A_{7p}A_{7p}^*A_{5p} + 2A_{9p}A_{9p}^*A_{5p}\\
&+ A_p^*A_{3p}^2e^{(-\beta_p+2\beta_{3p}-\beta_{5p})} + A_p^2A_{3p}e^{(2\beta_p+\beta_{3p}-\beta_{5p})}\\
&+ A_p^{2*}A_{7p}e^{(-2\beta_p-\beta_{5p}+\beta_{7p})} + A_{7p}^2A_{9p}^*e^{(-\beta_{5p}+2\beta_{7p}-\beta_{9p})}\\
&+ 2A_p^*A_{3p}^*A_{9p}e^{(-\beta_p-\beta_{3p}-\beta_{5p}+\beta_{9p})} + 2A_pA_{3p}^*A_{7p}e^{(\beta_p-\beta_{3p}-\beta_{5p}+\beta_{7p})}\\
&+ 2A_pA_{5p}^*A_{9p}e^{(\beta_p-2\beta_{5p}+\beta_{9p})} + 2A_{3p}A_{5p}^*A_{7p}e^{(\beta_{3p}-2\beta_{5p}+\beta_{7p})}\\
&+ 2A_{3p}A_{7p}^*A_{9p}e^{(\beta_{3p}-\beta_{5p}-\beta_{7p}+\beta_{9p})}\Big]\\
\gamma_{7p}\frac{\partial A_{7p}(z)}{\partial z} = \frac{\beta_{nl}\beta_{7p}^2}{8I_C^2}\Big[&2A_pA_p^*A_{7p} + 2A_{3p}A_{3p}^*A_{7p} + 2A_{5p}A_{5p}^*A_{7p} + A_{7p}A_{7p}^*A_{7p} + 2A_{9p}A_{9p}^*A_{7p}\\
&+ A_p^2A_{5p}e^{(2\beta_p+\beta_{5p}-\beta_{7p})} + A_pA_{3p}^2e^{(\beta_p+2\beta_{3p}-\beta_{7p})}\\
&+ A_{3p}^*A_{5p}^2e^{(-\beta_{3p}+2\beta_{5p}-\beta_{7p})} + A_p^{*2}A_{9p}e^{(-2\beta_p-\beta_{7p}+\beta_{9p})}\\
&+ 2A_p^*A_{3p}A_{5p}e^{(-\beta_p+\beta_{3p}+\beta_{5p}-\beta_{7p})} + 2A_pA_{3p}^*A_{9p}e^{(\beta_p-\beta_{3p}-\beta_{7p}+\beta_{9p})}\\
&+ 2A_{3p}A_{5p}^*A_{9p}e^{(\beta_{3p}-\beta_{5p}-\beta_{7p}+\beta_{9p})} + 2A_{5p}A_{7p}^*A_{9p}e^{(\beta_{5p}-2\beta_{7p}+\beta_{9p})}\Big]\\
\gamma_{9p}\frac{\partial A_{9p}(z)}{\partial z} = \frac{\beta_{nl}\beta_{9p}^2}{8I_C^2}\Big[&2A_pA_p^*A_{9p} + 2A_{3p}A_{3p}^*A_{9p} + 2A_{5p}A_{5p}^*A_{9p} + 2A_{7p}A_{7p}^*A_{9p} + A_{9p}A_{9p}^*A_{9p}\\
&+ A_p^2A_{7p}e^{(2\beta_p+\beta_{7p}-\beta_{9p})} + A_p^*A_{5p}^2e^{(-\beta_p+2\beta_{5p}-\beta_{9p})} + A_{5p}^*A_{7p}^2e^{(-\beta_{5p}+2\beta_{7p}-\beta_{9p})}\\
&+ 2A_pA_{3p}A_{5p}e^{(\beta_p+\beta_{3p}+\beta_{5p}-\beta_{9p})} + 2A_p^*A_{3p}A_{7p}e^{(-\beta_p+\beta_{3p}+\beta_{7p}-\beta_{9p})}\\
&+ 2A_{3p}^*A_{5p}A_{7p}e^{(-\beta_{3p}+\beta_{5p}+\beta_{7p}-\beta_{9p})} + \frac{1}{3}A_{3p}^3e^{(3\beta_{3p}-\beta_{9p})}\Big]
\end{aligned}
\tag{5}
$$

which can be solved numerically to probe the generation of the harmonic tones up to the ninth harmonic.

2.1 Analytical Solutions with Undepleted Pump Assumption

In principle, one could truncate the formulation presented above at the third harmonic and solve the coupled mode equations (CME) analytically using the undepleted pump assumption, similar to the derivation of a TWPA.[12,13] Although this approach is unrealistic, since the main aim of a TWPaM is to fully utilise the pump power to generate the desired harmonic tone, it could still provide valuable insights into the interaction between the primary pump tone and the third harmonic, particularly regarding the phase-matching condition.

By modifying Eq. 3 to take into account only the pump and its third harmonic, and assuming that the amplitude of the pump throughout the transmission line is much stronger than the third harmonic wave $A_p \gg$

A_{3p}, we arrive at:

$$\begin{aligned}\gamma_p \frac{\partial A_p(z)}{\partial z} &= \frac{\beta_{nl}\beta_p^2}{8I_C^2} A_p A_p A_p^* e^{-2\alpha_p z} \\ \gamma_{3p} \frac{\partial A_{3p}(z)}{\partial z} &= \frac{\beta_{nl}\beta_{3p}^2}{8I_C^2} \left[2A_p A_p^* A_{3p} e^{-2\alpha_p z} + \frac{1}{3} A_p^3 e^{(-3\alpha_p + \alpha_{3p})z} e^{-i\Delta_{\beta 3} z} \right].\end{aligned} \tag{6}$$

Solving this set of CME will results in: $A_p(z) = A_p 0 e^{i\varphi_p z}$, where $\varphi_p = -i\frac{\beta_{nl}\beta_p^2}{8I_C^2\gamma_p}(\frac{\varphi_{pp}}{2})$ and $\frac{\varphi_{pp}}{2} = |A_p 0|^2 e^{-2\alpha_p z}$; and

$$\frac{\partial a_{3p}(z)}{\partial z} - i\kappa_{3p} e^{i\Delta_{\phi 3} z} = 0 \tag{7}$$

where $\kappa_{3p} = \varphi'_{3p} Ap0 e^{(-\alpha_p + \alpha_{3p})z}$, $\varphi'_{3p} = \frac{\varphi_{3p}}{6}$ and, $\Delta_{\phi 3} = \Delta_{\beta 3} - 3\varphi_p + \varphi_{3p}$, which would have a solution in the form of:

$$a_{3p}(z) = \frac{(1 - e^{i\Delta_{\phi 3} z})\kappa_{3p}}{\Delta_{\phi 3}}. \tag{8}$$

From Eq. 8, it is evident that the growth of the third harmonic is maximised when $\Delta_{\phi 3} \to 0$. Therefore, we can employ the same phase-matching techniques used in the design of TWPA, such as periodic impedance loading[14] or coupled resonators[15] schemes, to maximise the third harmonic gain. Perhaps less apparent is the fact that the amplitude of the third harmonic is periodic depending on the length of the device, unlike in the case of a TWPA.

3. TRAVELLING WAVE PARAMETRIC TRIPLER

The framework formulated above can be utilised to simulate various TWPaM designs employing superconducting transmission media exhibiting Kerr-3 nonlinearity, such as kinetic-inductance based, Josephson junction-based, or symmetric-SQUID based mediums, similar to the formulation presented in Navarro et. al.[11] In this manuscript, we focus on the design of a parametric tripler using a niobium titanium nitride (NbTiN) kinetic-inductance based TWPaM as an example to showcase the methodology. A long transmission line comprising NbTiN thin film has been successfully demonstrated as a TWPaM previously,[5] but their operation was limited to a narrow frequency window. Our aim here is to demonstrate that it is indeed possible to design a TWPaM as a broadband tunable frequency multiplier, targeting broadband applications.

Our TWPaM-tripler design is based on inverted microstrip structure with the current carrying layer made out of NbTiN film of 35 nm thickness, with normal resistance expected to be 200 µΩcm. The transmission line is topped with 100 nm amorphous silicon as dielectric layer before a 200 nm niobium sky plane is deposited. The whole structure is supported with a 100 µm high resistivity silicon substrate. Fig. 1(a) shows the dimension of the unit cell making up the entire TWPaM with 300 of these unit cells cascaded. The length and spacing of the stubs were chosen to achieve 50 Ω characteristic impedance while having extra dispersion from around 40 GHz to suppress unwanted harmonics higher than the third harmonic. The length of the stubs are modified sinusoidally at ±5.5% to create a stopband near 10 GHz for phase-matching purposes. Before venturing into the mm/sub-mm range for more realistic application, we aim to demonstrate the operational principle of the TWPaM at the easier to operate microwave range with the generated third harmonic tone between 15–30 GHz.

3.1 Dispersion Engineering for Maximum Conversion Efficiency with the Analytical Solution

To investigate the effect of phase-matching on the efficiency of third harmonic generation, we utilise the analytical solution presented in Sec. 2.1. It is evident that high conversion efficiency can be achieved using the phase-matching technique, but the exponential growth of the third harmonic wave can only occur when the pump is placed near the dispersion-engineered stopband region that has the optimal phase-matching condition.[16] In other words, with this configuration, the operational bandwidth would be narrower than anticipated. This intrinsically narrow operational bandwidth is dictated by the need for the pump to be very close to the stopband frequencies,

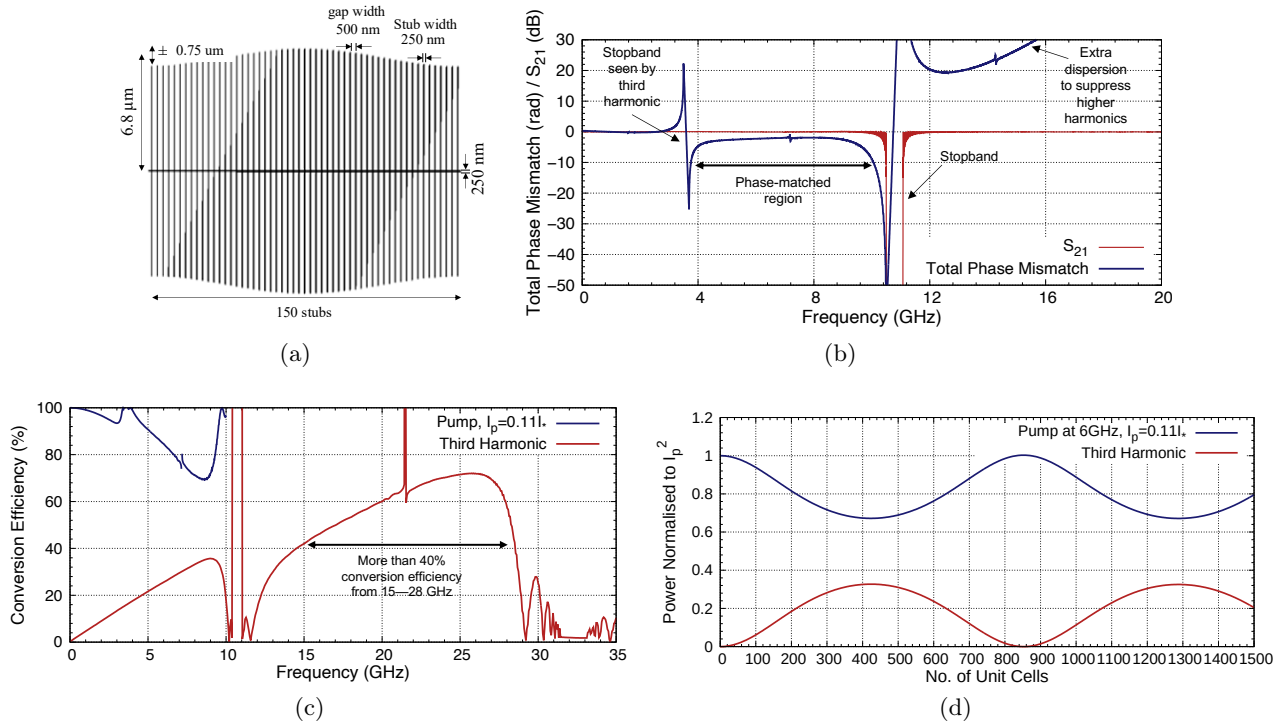

Figure 1. (a) The layout and dimensions of the unit cell within the TWPaM. (b) The wave-vector of the TWPaM, highlighting the dispersion engineering scheme employed to create stopbands for phase-matching and suppress higher harmonics. (c) Conversion efficiency of the TWPaM in terms of current amplitudes, demonstrating its broadband nature. (d) Power conversion efficiency in terms of the number of unit cells, determined using analytical solutions.

which are generally set with a very high quality factor to narrow down the zero-gain gap region in the case of TWPA. Therefore, to broaden the operational bandwidth, we can reduce the Q-factor of the stopband.

Furthermore, due to the third harmonic wave generated along the transmission line, the primary stopband will induced a lower resonance at a third of the fundamental frequency in the total dispersion relation. This, in effect, alters the $\Delta_{\phi 3}$ value between the two stopbands. If the Q-factor is low enough, the two dispersion curves overlap at larger intermittent frequencies, creating a region where $\Delta_{\phi 3}$ is very close to zero. This is illustrated in Fig. 1(b). It is noteworthy that the phase relation $\Delta_{\phi 3}$ in this case also heavily relies on the natural cutoff frequency of the nonlinear transmission. It is preferable for the cutoff to be set at a higher frequency so that the $\Delta_{\phi 3}$ curve is flatter near the operational frequencies (note the notch near the centre of the band in Fig. 1(b)), making it easier to achieve $\Delta_k \to 0$ at a broader bandwidth. The downside of this approach is that it promotes the growth of subsequent higher harmonics, such as the fifth, seventh, and ninth, thereby deteriorating the maximum energy transfer from the pump to the desired third harmonic. Therefore, there is a balance between widening the bandwidth and suppressing unwanted harmonics. There may be other design schemes to phase-match higher-than-third harmonics, such as the ninth harmonic, while suppressing other unwanted tones, but this is beyond the scope of this manuscript.

Fig. 1(c) shows the conversion efficiency of the TWPaM, calculated using the amplitude of the third harmonic current compared to the pump current wave, based on the analytical solution. As can be seen, the model predicts more than 40% operational bandwidth with a conversion efficiency better than 40% from 5-9 GHz, resulting in the generation of an output signal from about 15–27 GHz. Fig. 1(d) shows the total power conversion from the pump to the third harmonic in terms of device length, demonstrating the periodic behaviour as expected by Eq. 8.

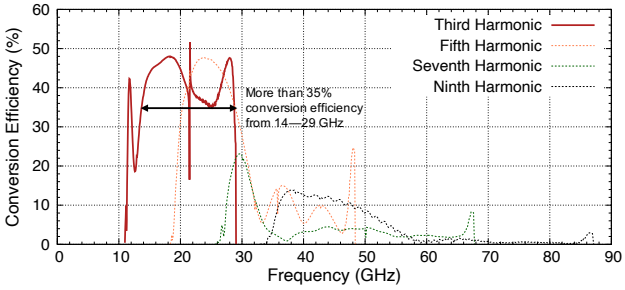

(a)

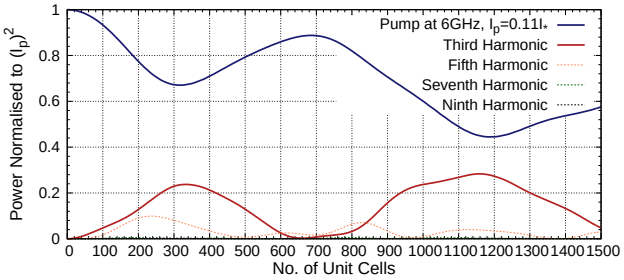

(b)

Figure 2. (a) Conversion efficiency of the TWPaM in terms of current amplitudes for harmonics up to the ninth. (b) Power conversion efficiency in terms of the number of unit cells for harmonics up to the ninth.

3.2 Numerical Solutions without Undepleted Pump Assumption

Having established the design of the TWPaM-tripler by minimising phase mismatch via dispersion-engineered stopbands, we now re-simulate the results using the full CME formulation, including harmonic tones up to the ninth without the pump-depletion assumption. It is expected that the simulated results will deviate from the previous simulation, which assumed an undepleted pump condition and did not include higher-than-third harmonics. Nevertheless, as shown in Fig. 2(a), we are still expected to achieve similar conversion efficiency across a broad bandwidth using the more realistic numerical model. The wave-amplitude conversion efficiency drops by about 5% to approximately 35% (due to the transfer of energy from the pump to the higher harmonics that are not fully suppressed) across a similar broad bandwidth from 14–29 GHz, which is not too far off from the prediction using the analytical solution.

From Fig. 2(a), it is evident that the generation of unwanted higher harmonics is also suppressed to a certain degree from 33 GHz onwards, thereby promoting the energy transfer from the pump to the primary desired third harmonic tone. It is clear that such a methodology is not ideal, as the fifth harmonic remains strong below 30 GHz, but this is inevitable due to the broad operational bandwidth we are targeting (3:1). Therefore, it is unavoidable that the lower half of the fifth harmonic band will overlap with the upper half of the third harmonic. Above 30 GHz, there is still the generation and growth of unwanted higher harmonics due to the gradual increase in dispersion of our transmission line, hence not fully suppressing their generation and growth, but weakening them significantly.

Finally, in Fig. 2(b), we show the power conversion efficiency from the pump to all harmonics up to the ninth in terms of device length, simulated with the pump set at 6 GHz. Here, it can be observed that the maximum third harmonic growth occurs at about 300-unit cell length, thus confirming the design of our TWPaM-tripler. More importantly, it is evident that the growth of the fifth harmonic is beyond its peak, whereas the generation of other higher harmonics is nearly negligible. There is indeed room for improvement to find an architecture where one can maximise third harmonic generation while ensuring the fifth harmonic is at its minimum, and other higher harmonics are suppressed. For example, at a length of about 1,160 unit cells, we can observe that the third harmonic power generation is higher, while the fifth and remaining higher harmonics are much weaker, albeit at the cost of nearly 4× longer device length.

4. CONCLUSION

We have presented a theoretical model for developing a superconducting frequency up-converter using SPA technology with a broad operational bandwidth, achieving close to 35% conversion efficiency over approximately 40% bandwidth. We fine-tune the dispersion relation of the nonlinear transmission line to enable phase-matching as well as for the suppression of higher unwanted harmonics to achieve high conversion efficiency. Although demonstrated at the microwave regime for ease of experimental setup and measurement, the same scheme can be applied to higher frequency ranges, extending into the millimetre range. There is also the possibility to cascade several of these TWPaM devices to reach even higher frequencies in the sub-millimetre range.

ACKNOWLEDGMENTS

This research was funded in part by the European Research Council (ERC) under the European Union's Horizon 2020 research and innovation programme with grant agreement No. [803862] (Project SPA4AstroQIT), the MERAC Foundation and the STFC Quantum for Science Grant (ST/Y004973/1). For the purpose of Open Access, the author has applied a CC BY public copyright license to any Author Accepted Manuscript version arising from this submission.

REFERENCES

[1] Hesler, J., Song, H., and Nagatsuma, T., "Terahertz schottky diode technology," in [*Handbook of terahertz technologies: Devices and applications*], (5), 104–131, Pan Stanford Publishing (2015).

[2] Mehdi, I., Siles, J. V., Lee, C., and Schlecht, E., "Thz diode technology: Status, prospects, and applications," *Proceedings of the IEEE* **105**(6), 990–1007 (2017).

[3] Klimovich, N., Day, P., Shu, S., Eom, B. H., Leduc, J., and Beyer, A., "Demonstration of a quantum noise limited traveling-wave parametric amplifier," *arXiv preprint arXiv:2306.11028* (2023).

[4] Qiu, J. Y., Grimsmo, A., Peng, K., Kannan, B., Lienhard, B., Sung, Y., Krantz, P., Bolkhovsky, V., Calusine, G., Kim, D., et al., "Broadband squeezed microwaves and amplification with a josephson travelling-wave parametric amplifier," *Nature Physics* **19**(5), 706–713 (2023).

[5] Cunnane, D., Leduc, H. G., Klimovich, N., Faramarzi, F., Beyer, A., and Day, P., "High-efficiency ka-band frequency multiplier based on the nonlinear kinetic inductance in a superconducting microstrip," *Applied Physics Letters* **124**(2) (2024).

[6] Klimovich, N., Wood, S., Day, P. K., and Tan, B.-K., "Investigating the effects of sum-frequency conversions and surface impedance uniformity in traveling wave superconducting parametric amplifiers," *Journal of Applied Physics* **135**(12) (2024).

[7] Macklin, C., O'brien, K., Hover, D., Schwartz, M., Bolkhovsky, V., Zhang, X., Oliver, W., and Siddiqi, I., "A near–quantum-limited josephson traveling-wave parametric amplifier," *Science* **350**(6258), 307–310 (2015).

[8] Planat, L., Dassonneville, R., Martínez, J. P., Foroughi, F., Buisson, O., Hasch-Guichard, W., Naud, C., Vijay, R., Murch, K., and Roch, N., "Understanding the saturation power of josephson parametric amplifiers made from squid arrays," *Physical Review Applied* **11**(3), 034014 (2019).

[9] Miano, A., Liu, G., Sivak, V., Frattini, N., Joshi, V., Dai, W., Frunzio, L., and Devoret, M., "Frequency-tunable kerr-free three-wave mixing with a gradiometric snail," *Applied Physics Letters* **120**(18) (2022).

[10] Tan, B.-K., Boussaha, F., Chaumont, C., Longden, J., and Montilla, J. N., "Engineering the thin film characteristics for optimal performance of superconducting kinetic inductance amplifiers using a rigorous modelling technique," *Open Research Europe* **2** (2022).

[11] Navarro Montilla, J. and Tan, B.-. K., "Generalising the Coupled-Mode Framework for Symmetric Travelling Wave Parametric Amplifiers with χ_3 Nonlinearity," *Applied Physics Letter* (2024). under review.

[12] Chaudhuri, S., Gao, J., and Irwin, K., "Simulation and analysis of superconducting traveling-wave parametric amplifiers," *IEEE Transactions on Applied Superconductivity* **25**(3), 1–5 (2014).

[13] O'Brien, K., Macklin, C., Siddiqi, I., and Zhang, X., "Resonant phase matching of josephson junction traveling wave parametric amplifiers," *Physical review letters* **113**(15), 157001 (2014).

[14] Chaudhuri, S., Li, D., Irwin, K., Bockstiegel, C., Hubmayr, J., Ullom, J., Vissers, M., and Gao, J., "Broadband parametric amplifiers based on nonlinear kinetic inductance artificial transmission lines," *Applied Physics Letters* **110**(15) (2017).

[15] White, T., Mutus, J., Hoi, I.-C., Barends, R., Campbell, B., Chen, Y., Chen, Z., Chiaro, B., Dunsworth, A., Jeffrey, E., et al., "Traveling wave parametric amplifier with josephson junctions using minimal resonator phase matching," *Applied Physics Letters* **106**(24) (2015).

[16] Tan, B.-. K., "A Josephson-Junction Travelling Wave Parametric Tripler," in [*Proc. 33rd Int. Sym. Space THz Technol. (ISSTT)*], (2024). .